

Vibrationally resolved core-photoelectron spectroscopy as an infinite-slit interferometry

Faris Gel'mukhanov,* P. Safek, and Hans Ågren

Theoretical Chemistry, Royal Institute of Technology, S-10044 Stockholm, Sweden

(Received 22 December 2000; published 12 June 2001)

During a molecular vibration, an atom changes continuously its position. Just as the emitted photoelectron waves, the electromagnetic waves absorbed by the atom in the different positions are strictly coherent and have different well-defined phases. These phases depend on the relation between the instantaneous internuclear distance and the photoelectron, respectively, photon wavelengths. We predict that the interference of these coherent waves strongly influences the vibrational profile of the photoelectron spectra of core electrons in a molecule. This effect increases with increasing x-ray photon frequency and results in a deformation and broadening of the vibrational profile. In the case of surface adsorbed molecules, the vibrational profile depends strongly on the direction of the photoelectron ejection and photon momentum, and the orientational sensitivity of a vibrational profile can even be used as a tool to define the orientation of adsorbed molecules.

DOI: 10.1103/PhysRevA.64.012504

PACS number(s): 33.60.Fy, 33.60.Cv, 32.30.-r, 79.60.-i

Core-level x-ray photoelectron spectroscopy (XPS) enables us to observe directly the influence of the chemical surroundings due to the chemical shift [1]. The spectral shape of XPS gives additional chemical information because different chemical states can change significantly the XPS vibrational fine structure [2]. X-ray photoelectron spectroscopy is also capable in resolving the vibrational fine structure in the core-level bands of adsorbates [3,4]. The conventional treatment of the vibrational fine structure is based on the Franck-Condon (FC) principle: The intensity of a vibrational line is proportional to the squared overlap integral between vibrational wave functions of core excited and ground states (the FC factor: $|\langle n|0\rangle|^2$). According to this principle, the XPS vibrational profile does not depend on the photon frequency, except possibly for a narrow region in the vicinity of the photoionization threshold, where post-collision interaction is important [5]. A further reason for a frequency dependence may be the bond-length sensitivity of the electronic transition moment near a shape resonance. It is now known that the FC principle can break down in *resonant* spectra due to a large momentum of the photoelectron \mathbf{k} with a site-dependent phase of the photoelectron wave function [6–9]. We show in this paper that the generalized FC (GFC) principle formulated in Ref. [7] results in a qualitatively new effect for ordinary “direct” x-ray photoelectron spectroscopy, namely, strong frequency and angular dependences of the XPS vibrational profile.

We consider, for simplicity, x-ray photoionization of the $1s$ core orbital in atom A in the diatomic molecule AB . Due to the locality of the x-ray transition, the wave functions of the incident x-ray photon and photoelectron imply a phase factor in the electronic transition moment

$$e^{i(\mathbf{k}-\mathbf{p}) \cdot \mathbf{R}_A}, \quad (1)$$

which depends on the difference between the photoelectron (\mathbf{k}) and photon (\mathbf{p}) momenta and on the coordinate (\mathbf{R}_A

$= \alpha \mathbf{R}$) of the core ionized atom A with respect to the center of mass of the molecule. Here, $\alpha = \mu/m_A$ is the ratio of the reduced mass μ and the mass of atom A , m_A . The origin of the phase factor (1) may also be understood from Fig. 1. During nuclear vibrations, \mathbf{R}_A and, hence, the phase factor (1) continuously vary because of changes of the internuclear radius-vector \mathbf{R} . Therefore instead of a “2-slit” interference as shown for simplicity in Fig. 1, we have here an “infinite-slit interferometer” due to the continuous change of R .

It is not hard to see that the ordinary FC factor must be replaced in the x-ray region by the GFC factor [7]

$$F_{n0}(\mathbf{k}-\mathbf{p}) = |\langle n | e^{i\alpha|\mathbf{k}-\mathbf{p}|R \cos \theta} | 0 \rangle|^2. \quad (2)$$

When $|\mathbf{k}-\mathbf{p}| \cos \theta$ is large, the phase factor (1) produces a strong modulation of the integrand in the matrix elements at the right-hand side of Eq. (2). That is what makes the XPS vibrational profile ω dependent. Another prediction obtained from the GFC principle (2) is the strong anisotropy of the GFC factors: They depend on the angle θ between $\mathbf{k}-\mathbf{p}$ and the molecular axis, as well as on the angle between \mathbf{k} and \mathbf{p} .

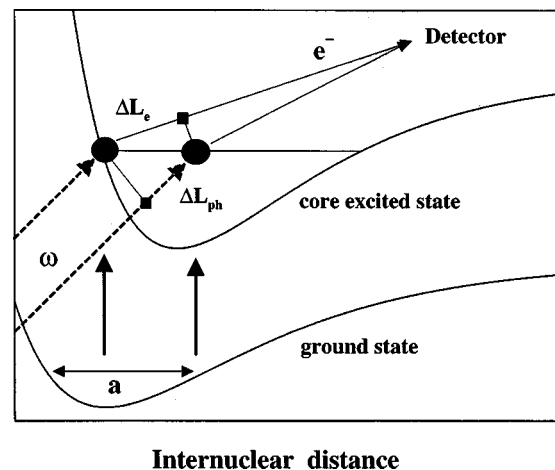


FIG. 1. Pictorial representation of absorption of electromagnetic waves and emission of electron waves by atoms in different internuclear positions.

*Permanent address: Institute of Automation and Electrometry, 630090 Novosibirsk, Russia.

This spectral feature is important for surface-adsorbed molecules where the molecules have a certain space orientation.

The problem is now reduced to that of evaluating the double differential cross section for the K photoionization of atom A :

$$\frac{d^2\sigma(\varepsilon, \omega)}{d\hat{\mathbf{k}}dE} = 4\pi p d^2 |\mathbf{e} \cdot \hat{\mathbf{k}}|^2 \sum_n \frac{F_{n0}(\mathbf{k}-\mathbf{p})\Gamma}{(\varepsilon - I_{1s} - \omega_{n0})^2 + \Gamma^2}. \quad (3)$$

Here, d is the electronic transition moment of the photoionization, $\hat{\mathbf{k}} = \mathbf{k}/k$, $\varepsilon = \omega - E$ is the binding energy, \mathbf{e} is the vector of photon polarization, $E = k^2/2$ is the photoelectron energy, $\omega_{n0} = \epsilon_n^c - \epsilon_0^0$ where ϵ_n^c and ϵ_0^0 are the vibrational energies of the core excited and ground states, respectively, Γ is the lifetime broadening of the core ionized state, and I_{1s} is the ionization potential of the $1s_A$ level. We use here atomic units. The only difference with the conventional formula is the GFC factor $|F_{n0}(\mathbf{k}-\mathbf{p})|^2$. To describe a real experimental situation, the cross section (3) has to be convoluted with the spectral function of the incident x-ray beam that has a finite spectral width. One should note that Eq. (3) is true only for fast photoelectrons, $kR \gg 1$. Otherwise, the transition dipole moment d becomes \mathbf{R} dependent and it must then also be included in the GFC factor (2).

Let us estimate the phase in Eq. (1), $\varphi = (\mathbf{k}-\mathbf{p}) \cdot \mathbf{R}_A = \varphi_e + \varphi_{ph}$, which consists of the electronic, $\varphi_e = k\alpha\Delta L_e$, and photon, $\varphi_{ph} = p\alpha\Delta L_{ph}$, contributions (see Fig. 1). The phase takes maximum value, $\varphi = (k+p)\alpha\Delta L_e \sim (k+p)\alpha a$, when the photoelectron is ejected in opposite direction relative to \mathbf{k} and $\theta = 0^\circ$. In this case, the path differences of the electron and the photon are the same and they are of the order of the size of the vibrational wave function: $\Delta L_e = \Delta L_{ph} \sim a \sim 0.1$. A typical value of α is ~ 0.5 . The electron and photon phases depend on ω differently and have different critical energies E_c and ω_c

$$\begin{aligned} \varphi_e &\approx \sqrt{\frac{\omega - I_{1s}}{E_c}}, & E_c &\approx \frac{1}{2(\alpha a)^2} \approx 5 \text{ keV}, \\ \varphi_{ph} &\approx \frac{\omega}{\omega_c}, & \omega_c &\approx \frac{137}{\alpha a} \approx 75 \text{ keV}. \end{aligned} \quad (4)$$

One can see that the electron phase factor becomes important ($\varphi_e \geq 1$) for photoelectron energies $\omega - I_{1s} \geq 5$ keV. The photon phase is close to unity for larger photon energies $\omega \geq 75$ keV. We will see, however, that the photon phase begins to influence the XPS vibrational profile even for smaller photon energies ($\omega \sim 10$ keV).

To perform numerical simulations, we follow two techniques. The first one is the direct implementation of the time-independent Eq. (3) where only bound-bound vibrational transitions are included. The second one is the time-dependent wave-packet method, taking into account both bound-bound and bound-continuum transitions as outlined in Ref. [7]. Both these approaches led to the same results for the CO molecule. This means that bound-continuum transitions are negligible in the studied energy range.

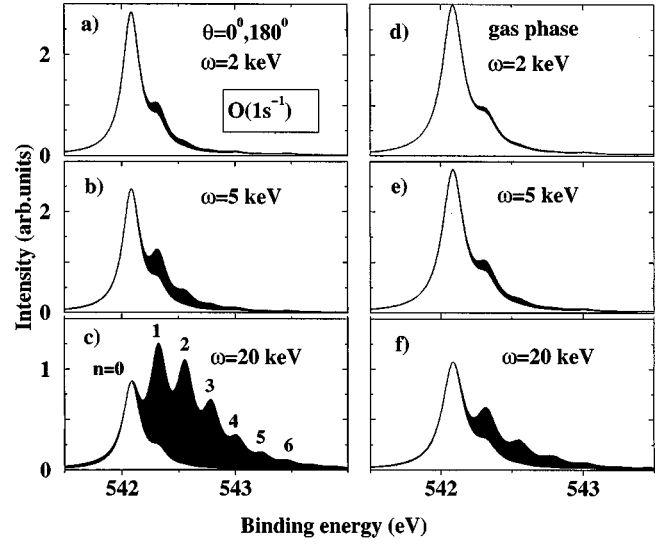


FIG. 2. Oxygen K -level photoelectron spectra of CO for different photon energies. $\mathbf{k} \uparrow \downarrow \mathbf{p}$. Left panels (a,b,c) show the spectra for photoelectrons ejected parallel to the molecular axis. The case of randomly oriented molecules is shown in panels (d,e,f). The unfilled plots show the spectra calculated without phase factor $\exp[i\alpha(\mathbf{k}-\mathbf{p}) \cdot \mathbf{R}]$ (their XPS intensities are reduced to have the same intensity of the low-energy peak as the shaded spectra). The shaded plots are calculated making use of the GFC factors. The adiabatic O $1s$ ionization potential (0-0 transition) is equal to 542.1 eV.

The simulated profiles of O $1s$ and C $1s$ photoelectron spectra of oriented and randomly oriented CO molecules are shown in Fig. 2 and Fig. 3, respectively. The calculations were performed for a monochromatic x-ray beam. The GFC and FC factors are calculated, making use of the spectroscopic constants of the Morse potential-energy curves of ground and core ionized states of CO in gas phase [5,10]. The lifetime width Γ used in the simulations is 0.09 eV for

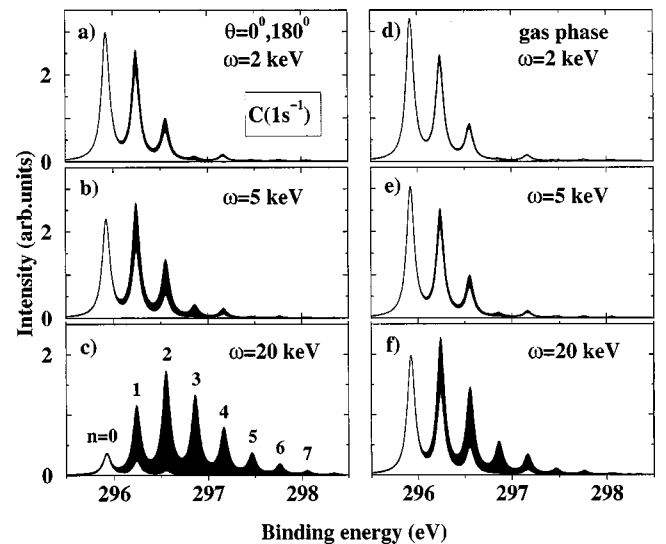


FIG. 3. Carbon K -level photoelectron spectra of CO for different photon energies. $\mathbf{k} \uparrow \downarrow \mathbf{p}$. Other notations are the same as in Fig. 2. The adiabatic C $1s$ ionization potential (0-0 transition) is equal to 295.9 eV.

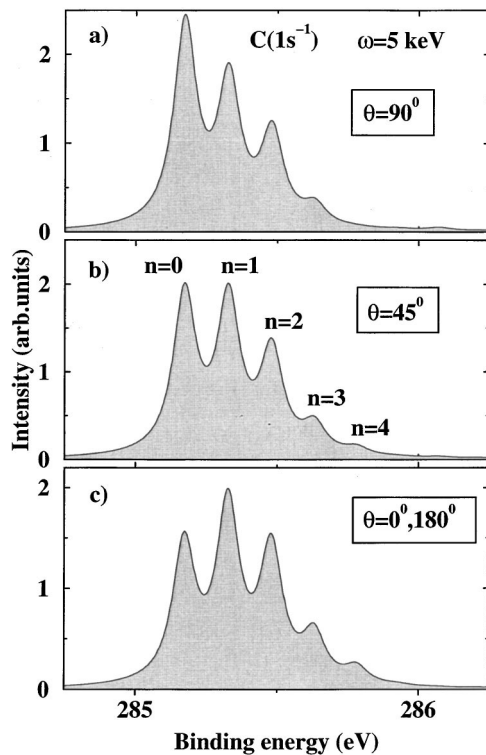


FIG. 4. Carbon K -level photoelectron spectra of CO for different angles θ between \mathbf{k} and the molecular axis: $\mathbf{k}\downarrow\mathbf{p}$. Input data for CO adsorbed in upright position on hollow site in the $c(2\sqrt{2}\times\sqrt{2})R45^\circ\text{CO}/\text{H}/\text{Ni}(100)$ superstructure [4]. The adiabatic C $1s$ ionization potential (0-0 transition) is equal to 282.5 eV.

the O $1s^{-1}{}^2\Sigma^+$ state and 0.0485 eV for the C $1s^{-1}{}^2\Sigma^+$ state [10]. The figures show that the GFC factors begin to modify the spectra essentially when $\omega\approx 2-5$ keV. When the electron phase crosses π ($\omega\approx 15$ keV) the phase factor (1) changes the spectra drastically: It produces both a shift of the center of gravity and a broadening of the spectra. Both O $1s$ and C $1s$ spectra show suppression of the strongest 0-0 vibrational line when ω increases. The gas-phase molecules are totally disordered so the XPS cross section (3) has to be averaged over all molecular orientations (over angle θ). Comparison of spectra of oriented and disordered CO molecules (left and right columns in Figs. 2 and 3) show that the role of the GFC factors is larger for oriented molecules. This is explained by a suppression up to zero of the phase $\varphi = \alpha|\mathbf{k}-\mathbf{p}|R \cos \theta$ in Eq. (2) when $\theta\rightarrow 90^\circ$.

Surface adsorption gives a way to study the role of molecular orientation. To simulate the C $1s$ x-ray photoelectron spectra of adsorbed CO, we used the spectroscopic constants from Ref. [4], which reports vibrationally resolved O($1s^{-1}$) and C($1s^{-1}$) XPS spectra of CO adsorbed in the upright position on a hollow site with the carbon end down in the $c(2\sqrt{2}\times\sqrt{2})R45^\circ\text{CO}/\text{H}/\text{Ni}(100)$ superstructure at $\omega = 700$ eV and $\omega = 320$ eV, respectively. Figure 4 shows the sensitivity of the XPS profile to the orientation of the photoelectron momentum relative to the molecular axis. When the photon energy increases, the direction of the photon momentum becomes important, Fig. 5. Apparently, the dependence of the spectral profile on the mutual orientations of \mathbf{k} and \mathbf{p}

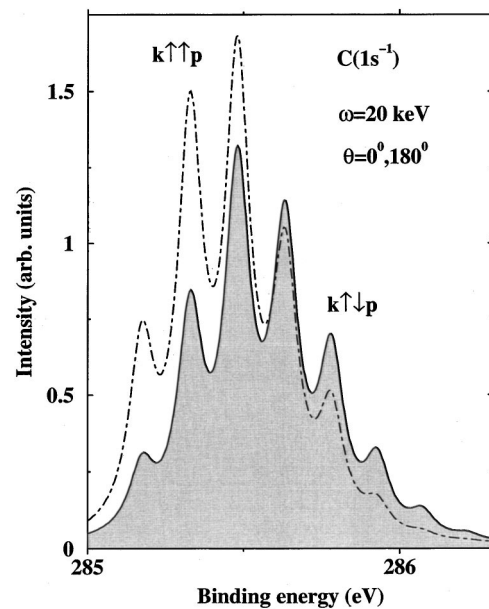


FIG. 5. Carbon K -level photoelectron spectra of CO for different orientations of electron and photon momenta: $\mathbf{k}\uparrow\uparrow\mathbf{p}$ and $\mathbf{k}\downarrow\uparrow\mathbf{p}$. Other data are the same as in Fig. 4.

takes place also for randomly oriented molecules. The sensitivity of the vibrational profile to the orientation of \mathbf{k} and \mathbf{p} , relative to the axis (or plane) of molecular vibrations, can be used to determine the orientation, as well as the degree of orientation of the adsorbed molecules.

The observation of the discussed effects are certainly possible using the modern techniques of high-energy x-ray photoelectron spectroscopy. As one can realize from Figs. 2 and 3, the increase of the photon energy leads to a broadening and shift of the center of gravity of the vibrational profile of the order ~ 0.5 eV. This means that the bandpass of the incident radiation and spectral resolution of the electron spectrometer should go below 0.5 eV. This is feasible considering, for example, that x-rays with a 5 meV bandpass were obtained for $\omega = 13.84$ keV in Ref. [11], and that XPS experiments using high-energy Cr $K\beta$ radiation (5946.86 eV) can be conducted as reported in Ref. [12]. Yet another relevant experiment to quote is the investigation of Ge $1s$ XPS in Ge and GeO_2 using high-energy synchrotron radiation (13.6 keV) with the photoelectron energies near 2.5 keV [13]. Using tunable high-flux monochromatized synchrotron radiation and a hemispherical electron analyzer, Grehk *et al.* [14] studied Auger emission ($E\approx 3$ keV) with the total-energy resolution, $\Delta E = 0.8$ eV and an x-ray beam bandwidth of 0.5 eV. Alternatively to electrostatic analyzers, electron time-of-flight spectrometers [15] can also be used for electrons with kinetic energies up to 5 keV and with a resolving power $E/\Delta E\sim 10^4$.

ACKNOWLEDGMENTS

We thank Professor J.-E. Rubensson for fruitful discussion of the experimental aspects of the high-energy XPS. This work was supported by the Wenner-Gren foundation.

- [1] K. Siegbahn, C. Nordling, G. Johansson, J. Hedman, P. F. Hedén, K. Hamrin, U. Gelius, T. Bergmark, L. O. Werme, R. Manne, and Y. Baer, *ESCA Applied to Free Molecules* (North-Holland, Amsterdam, 1969).
- [2] U. Gelius, S. Svensson, H. Siegbahn, E. Basilier, Å. Faxälv, and K. Siegbahn, *Chem. Phys. Lett.* **28**, 1 (1974).
- [3] J. Andersen, A. Beutler, S. L. Sorensen, R. Nyholm, B. Setlik, and D. Heskett, *Chem. Phys. Lett.* **269**, 371 (1997).
- [4] A. Föhlisch, N. Wassdahl, J. Hasselström, O. Karis, D. Menzel, N. Mårtensson, and A. Nilsson, *Phys. Rev. Lett.* **81**, 1730 (1998).
- [5] B. Kempgens, K. Maier, A. Kivimäki, H. M. Köppe, M. Neeb, M. N. Piancastelli, U. Hergenbahn, and A. M. Bradshaw, *J. Phys. B* **30**, 741 (1997).
- [6] F. Gel'mukhanov, H. Ågren, and P. Salek, *Phys. Rev. A* **57**, 2511 (1998).
- [7] P. Salek, F. Gel'mukhanov, H. Ågren, O. Björneholm, and S. Svensson, *Phys. Rev. A* **60**, 2786 (1999).
- [8] F. Gel'mukhanov and H. Ågren, *Phys. Rep.* **312**, 87 (1999).
- [9] O. Björneholm, M. Bässler, A. Ausmees, I. Hjelte, R. Feifel, H. Wang, C. Miron, M. N. Piancastelli, S. Svensson, S. L. Sorensen, F. Gel'mukhanov, and H. Ågren, *Phys. Rev. Lett.* **84**, 2826 (2000).
- [10] P. Skytt, P. Glans, K. Gunnelin, J.-H. Guo, J. Nordgren, Y. Luo, and H. Ågren, *Phys. Rev. A* **55**, 134 (1997).
- [11] M. Schwoerer-Böning, A. T. Macrander, and D. A. Arms, *Phys. Rev. Lett.* **80**, 5572 (1998).
- [12] C. G. Walker, S. A. Morton, N. M. D. Brown, and J. A. D. Matthew, *J. Electron. Spectrosc. Relat. Phenom.* **95**, 211 (1998).
- [13] V. Formoso, A. Filipponi, A. Di Cicco, G. Chiarello, R. Felici, and A. Santaniello, *Phys. Rev. B* **61**, 1871 (2000).
- [14] T. M. Grehk, W. Drube, R. Treusch, and G. Materlik, *J. Electron Spectrosc. Relat. Phenom.* **93**, 227 (1998).
- [15] O. Hemmers, S. B. Whitfield, P. Glans, H. Wang, D. W. Lindle, R. Wehlitz, and I. A. Sellin, *Rev. Sci. Instrum.* **69**, 3809 (1998).